Measurement of air resistance on an air track

Barbara S. Andereck

Department of Physics and Astronomy, Ohio Wesleyan University, Delaware, Ohio 43015

An extension of a standard air track experiment is described in which the effects of air resistance can be studied. A circular disk is placed on one end of an air track cart to provide air drag. The data analysis consists of subtracting the ''ideal'' velocity for a frictionless situation from the measured velocity and plotting the difference as a function of the ideal velocity. The resulting curve is fitted with a modified power-law and the coefficient of the cubic term is studied as a function of the area of the disk, a behavior that can be predicted theoretically. Frictional effects in addition to the air drag on the disk were found to be significant and were accounted for. © *1999 American Association of Physics Teachers.*

I. INTRODUCTION

Air tracks have provided physicists with an approximation of the idealized ''frictionless inclined plane'' for decades. With the introduction of motion sensors, the position, velocity, and acceleration of a cart on the air track can be monitored and students can see graphed what they often have trouble visualizing—a velocity curve whose slope does not change as the cart comes to a stop at the top of the air track and slides back down. Computerized collection of large data sets and analysis using commonly available software open up the possibility of investigating more than the idealized motion. Physics students at the introductory level or in a more advanced undergraduate laboratory course can detect and analyze the effects of frictional forces on the air track cart. Simple transformations of the data using a graphing package such as Easyplot™[1] allow the determination of the power-law dependence of the drag on velocity. The drag due to air resistance can be enhanced by attaching cardboard disks to one end of the cart.

This straightforward experiment and somewhat more involved analysis introduce the student to useful ideas beyond the routine inclined-plane phenomenon:

(1) What appears to be ''ideal'' behavior may not be upon closer examination.
(2) Small deviations from the ''ideal'' can be studied using approximations (an introduction to perturbation theory.)
(3) To see subtle effects we must subtract out the dominant behavior
(4) Physics works even for nonideal inclined planes!

Effects of air resistance have been explored by introductory students in a variety of ways. Often some variation of difference equations is used to predict the effect of air drag.[2] Or the results of the air drag are studied by looking at the terminal velocity[3] or the net effect on the motion.[4] An interesting experiment that more advanced undergraduates might perform was discussed by Basano and Ottonello.[5] They analyzed the position of a falling disk as a function of time and found that for large enough disk areas both an effective mass due to the air being dragged by the disk and a history effect were necessary to fit the data.

The experiment described in this paper has the unique feature of a direct analysis of the air resistance effects present in the data, by subtracting out the dominant, ''ideal''

behavior. It also differs from prior work in that its focus is on the behavior of the velocity, rather than the position, as a function of time.

II. THEORY OF MOTION ON THE INCLINED PLANE IN THE PRESENCE OF SLIDING FRICTION AND AIR RESISTANCE

Because sliding friction is more familiar to introductory physics students and mathematically simpler, I introduce the qualitative effects of drag on the air track cart with a discussion of the effect of sliding friction: For a frictionless incline the only net force on the cart is the component of its weight parallel to the track:

$$F_{\text{along the incline}} = -mg\sin\theta = m\frac{dv}{dt}, \tag{1}$$

where m is the mass of the cart, g is the acceleration due to gravity, θ is the angle of the incline, and down the incline (toward the motion sensor) is taken to be the negative direction. Since $g\sin\theta$ is a constant throughout the trip, the equation can be integrated to yield

$$v_{\text{ideal}} = v_0 - (g\sin\theta)t, \tag{2}$$

where v_0 is the velocity of the cart at $t=0$. The graph of the ideal velocity as a function of time is simply a straight line with slope $-g\sin\theta$ as shown by the solid line in Fig. 1.

Next consider the effect of a velocity-independent frictional force, F_μ. This force arises from sliding friction and is proportional to the normal force. The specific form of the force is not crucial for the analysis, only the fact that it is independent of the magnitude of the velocity and opposite in direction to the velocity. With this addition we have

$$F_{\text{along the incline}} = -mg\sin\theta \mp F_\mu = m\frac{dv}{dt}, \tag{3}$$

where $-F_\mu$ is the frictional contribution when the cart is moving up the inclined plane and $+F_\mu$ applies when the cart is moving down the air track. The velocity for the case where the cart is moving up the incline can be found by integrating Eq. (3):

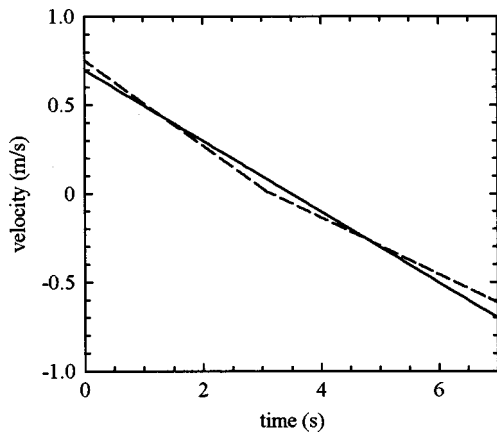$$v_{\text{up}} = v_0' - (g\sin\theta)t - \frac{F_\mu}{m}t, \tag{4}$$

Fig. 1. Velocity versus time for constant negative acceleration (solid line) as a cart moves up ($v > 0$) and down ($v < 0$) an air track compared to the case of acceleration in the presence of an additional velocity-independent frictional force (dashed line).

where v_0' is the velocity at $t=0$, which might differ from v_0 in the case of the trip without friction. The effect of the sliding friction is to steepen the slope of the v versus t graph for $v > 0$. Similarly, the magnitude of the slope will be reduced for the case when $v < 0$ (the cart is sliding down the incline). With the slope given by $-g \sin \theta + F_\mu/m$ the downward part of the velocity versus time graph begins when $v = 0$. The behavior of the velocity for the full trip in the presence of friction is shown by the dashed line in Fig. 1. Note that in the figure v_0' has been chosen to be larger than v_0 in order to allow the slope of the ideal velocity curve to approximate the acceleration for the round trip.

To this point the mathematics and the concepts should be familiar to students of introductory physics, in either an algebra- or calculus-based course. The extension of the discussion to a velocity-dependent drag force requires more sophisticated mathematics, but the concept is analogous to the sliding friction case. Students who have followed the previous argument should be primed to tackle the air-resistance case, either working through all the mathematics (if they have a calculus background) or taking a few mathematical leaps of faith along the way.

Consider the case of a velocity-dependent drag of the form $F_{\text{drag}} = \mp b|v|^n$, where the sign is chosen so that the drag force is opposite the direction of the velocity. Now the total force on the cart is velocity dependent and in the absence of the sliding friction term has the form

$$F_{\text{along the incline}} = -mg \sin \theta \mp b|v|^n = m \frac{dv}{dt}, \quad (5)$$

which leads to a differential equation for v beyond the scope of most general physics students. But the acceleration is again dominated by the constant component of the acceleration due to gravity along the plane if $b|v|^n \ll mg \sin \theta$, so we will approximate the velocity in the drag term by the ideal velocity from Eq. (2). This leads to the more manageable equation for v:

$$\frac{dv}{dt} = -g \sin \theta \mp \frac{b}{m} |v_0 - (g \sin \theta)t|^n. \quad (6)$$

This equation is readily integrated to yield

$$v = v_0' - (g \sin \theta)t$$

$$+ \frac{b}{(n+1)mg \sin \theta} [|v_0 - (g \sin \theta)t|^{n+1} - |v_0|^{n+1}] \quad (7)$$

or

$$v - v_{\text{ideal}} = (v_0' - v_0) + b'[|v_{\text{ideal}}|^{n+1} - |v_0|^{n+1}],$$

where

$$b' = \frac{b}{(n+1)mg \sin \theta}. \quad (8)$$

Note that the $\mp$ in Eq. (6) disappeared in Eq. (7) due to the integration of the expression involving the absolute value.

Equation (6) can be integrated directly in the case where $n=2$. When the cart is moving up the inclined plane, the result of integrating is

$$\tan^{-1} \left(\frac{bv^2}{mg \sin \theta} \right)^{1/2} - \tan^{-1} \left(\frac{bv_0^2}{mg \sin \theta} \right)^{1/2} = - \left(\frac{bg \sin \theta}{m} \right)^{1/2} t. \quad (9)$$

In the limit that $bv \ll g \sin \theta$, the arc tangents can be expanded to third order in their arguments and the equation rearranged to yield

$$v \approx v_0 - g \sin \theta t + \frac{b}{3mg \sin \theta} (v^3 - v_0^3), \quad (10)$$

which is identical to Eq. (7) when $n=2$, except that the actual velocity v rather than the ideal velocity, $v_0 - g \sin \theta t$, appears in the last term on the right-hand side. Equations (10) and (7) agree to third order in $bv^2/mg \sin \theta$. When the cart is moving down the incline the integrated solution to Eq. (6) involves the inverse hyperbolic tangent instead of the inverse tangent. In the case of the cart moving both up and down the air track, $t \neq 0$ at the top of the trajectory, making the limits on the integral less straightforward. To yield a solution most symmetric with the upward case, we can integrate from an arbitrary time t to the final time and use the final velocity rather than the initial velocity in the solution:

$$\tanh^{-1} \left(\frac{bv_f^2}{mg \sin \theta} \right)^{1/2} - \tanh^{-1} \left(\frac{bv^2}{mg \sin \theta} \right)^{1/2}$$

$$= - \left(\frac{bg \sin \theta}{m} \right)^{1/2} t. \quad (11)$$

The velocity at the end of the trip will be approximately equal to the initial velocity, as the cart started up the incline. Also, the expansion of the inverse hyperbolic tangent differs in sign from the expansion for the arc tangent in the third-order term. Thus we can combine Eqs. (10) and (11) into one equation that has the form of Eq. (7).

III. SETUP AND DATA COLLECTION

The experimental setup consists of a computer, a motion sensor (I used the motion sensor and motion plotter associated with the Pasco interface), an air track (2 m in length in this case) and cart, cardboard, and small weights. The air track is leveled and then tilted roughly a hundredth of a radian (using aluminum shims). The motion sensor is mounted beyond one end of the air track (I chose the bottom end), and the position of the cart is monitored as it slides freely up the incline, stops, and slides back down. Data can be collected for a ''bare'' cart, or a piece of cardboard can be mounted on one end of the cart to provide detectable air
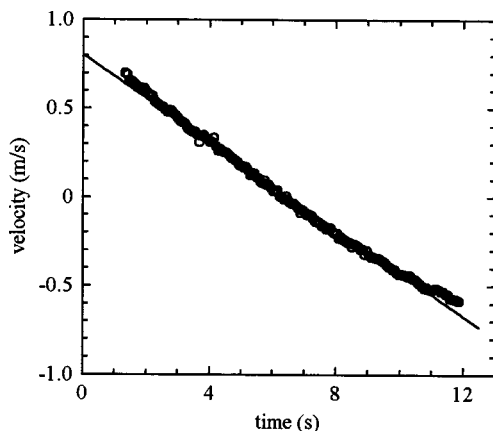
Fig. 2. Velocity versus time data (circles) for a cart carrying a disk of area 0.020 m². The best linear fit to the data (solid line) is $v = -0.123t + 0.804$.

Fig. 3. Transformed data for the 0.020-m² disk showing deviation from ideal velocity versus ideal velocity. The data are fit using the equation $y = B*\text{abs}(x+C)^3 + E$. The best fit (solid line) has $B = 0.313$ s²/m², $C = -0.00331$ m/s, and $E = -0.0209$ m/s.

resistance. If the goal of the experiment is to maximize air resistance and minimize contact friction, then the cardboard should be counterbalanced by attaching an equal mass to the opposite end of the cart. This procedure is recommended, so that the velocity deviation from ideal results more from air drag, rather than a combination of air drag and sliding friction. This in turn allows for simpler curve fits. Air drag will result from the presence of any reasonable-sized ($\gtrsim 0.01$ m²) piece of cardboard. If the dependence of the drag coefficient on area is to be studied, the cardboard should be circular (see discussion in Sec. VI) and data should be collected for a range of areas. A large circular piece of cardboard can be marked with circles that have areas decreasing in roughly equal increments. The cardboard can then be trimmed after each set of trials. Multiple trials for each area are recommended due to scatter in fitting results. It is also best to use the same air track for all runs. The effect of sliding friction can be maximized compared to air resistance by eliminating the cardboard entirely and weighting one end of the cart.

The motion sensor is activated and the cart is launched by hand at a speed that will allow the cart to approach but not strike the upper end of the air track. Data for one complete trip up the incline and back down are collected. The velocity of the cart is automatically determined by Pasco's Motion Plotter software from the distance data. This can be done with various levels of smoothing. Results presented in this paper were derived from velocity data with a smoothing of seven (the default value for Motion Plotter). The velocity data need to be edited to include only those values when the cart is moving *freely* up the incline and back down.

IV. ANALYSIS OF THE DATA

Once the data have been collected, they can be analyzed using a plotting package such as EasyPlot. First the velocity versus time data are graphed. As a reasonable approximation to the ideal velocity, a linear fit is made to the data. (See Fig. 2.) The predicted slope is $-g \sin \theta$. The slope from the curve fit is greater in magnitude than the theoretical value, with the deviation increasing with increasing air resistance. This deviation arises because the air resistance reduces the speed throughout the run. Thus there are larger speeds at the beginning of the rise up the incline than at the bottom on the way down. As we see from Eq. (5) the acceleration is greater
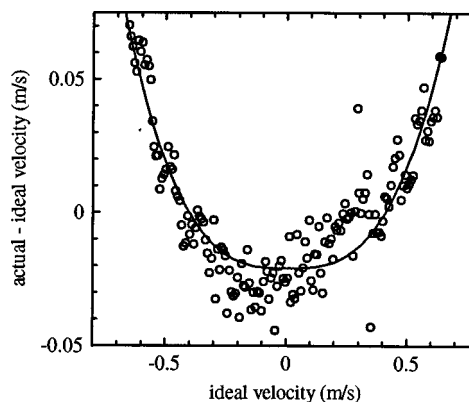
for larger magnitude velocities, hence the slope of the velocity versus time plot will be skewed to slightly higher values than the ''ideal'' acceleration in the presence of velocity-dependent forces.

The simple relationship expressed in Eq. (8) will enable us to find the power, n, and the coefficient $b = b'(n+1)mg \sin \theta$. To find these parameters we need a graph showing the difference between the observed velocity and the ideal velocity as a function of the ideal velocity. Such a graph can be obtained by transforming the velocity versus time graph twice. The first transformation converts the horizontal axis from ''time'' to ''ideal velocity.'' For the ideal velocity it is recommended that the curve fit equation be used (see Fig. 2), since the actual data deviate less from the curve fit than from the theoretical fit. The transformation equation needed for this step is $x \rightarrow mx + b$. (Note that m will be negative if the motion sensor is mounted at the bottom of the incline.) This first transformed curve represents actual velocity versus ideal velocity, and hence will be roughly linear, with unit slope. The curve is transformed again, this time using $y \rightarrow y - x$. This converts the vertical axis into ''actual minus ideal velocity,'' or ''deviation of velocity from ideal.'' The second transformed curve will be concave upward, with the type of curvature depending on the nature of the frictional force involved, the steepness (or shallowness) depending on the magnitude of the frictional force, and the scatter depending on the smoothness of the air track, the noise in the motion sensor, and the smoothness of the ''launch.'' (See Fig. 3 for an example of this type of curve.) Students should be asked to explain why the doubly transformed curve has so much scatter when the original (velocity versus time) curve was smooth. The magnification of the effect of noise seen with the subtraction of two nearly equal quantities can be used to reinforce the concept of *relative* uncertainty.

The final plot can be fitted in a number of ways, with anywhere from two to four adjustable parameters, using a fitting equation of the form

$$y = B*\text{abs}(x - C)^D + E. \tag{12}$$

From Eq. (8) it appears that C should be 0. There is, however, non-negligible air resistance and so the symmetry between the motion up and down the plane is broken; the initial velocity up the plane is greater than the final velocity (at the

same location) down the plane. This asymmetry systematically skews the slope of the velocity versus time curve to values greater in absolute value than $g \sin \theta$. Consequently, the fitted line is not tangent to the velocity versus time curve at the point of zero velocity. This skewing necessitates the use of an x-offset in Eq. (12). Because of the complexity of and approximations in the expressions included in the constant E, it is just taken to be an adjustable parameter in the curve fit. The most interesting fitting parameter is the overall coefficient B, which depends on the size and geometry of the object producing the drag. The B in Eq. (12) will be given theoretically by the b' in Eq. (8) if air drag on the cardboard disk is the only frictional force present. Finally, the exponent on the velocity can be studied. If the drag on the cart is purely due to contact friction, then $D = n + 1$ should be 1. The exponent in the case where drag is dominated by air resistance is discussed in the next section.

V. THEORY OF AIR DRAG

Some introductory texts mention the dependence of the drag force on velocity.[6] In the case of viscous flow for small bodies, the drag is proportional to the velocity. Stoke's Law for laminar flow around spheres is the classic example of this situation. But if the velocity is high and/or the viscosity is low, and/or the object is large enough, the drag force is proportional to the square of the velocity. The distinction between these two cases is made concrete by referring to the dimensionless Reynolds number R:

$$R = \frac{\rho L v}{\mu}, \tag{13}$$

where ρ is the density of the fluid through which the object is moving, L is a characteristic length associated with the cross section of the object, v is the relative velocity of the object and the fluid far from the object, and μ is the viscosity of the fluid. For Stoke's Law to hold we must have $R \lesssim 1$,[7] but for our cardboard moving through air the Reynolds number is approximately

$$R \approx \frac{1.2 \ \text{kg/m}^3 \times 0.1 \ \text{m} \times 0.3 \ \text{m/s}}{2 \times 10^{-5} \ \text{kg/m} \cdot \text{s}} \approx 2000, \tag{14}$$

so the small R approximation is clearly not applicable. In the limit of large Reynolds number, a bluff object, such as our cardboard, will experience a large pressure difference from front to back, which is closely approximated by the Bernoulli effect:[8]

$$p_{\text{front}} - p_{\text{back}} = \tfrac{1}{2} \rho v^2. \tag{15}$$

This pressure difference produces a drag force, F_D:

$$F_D = C_D A \tfrac{1}{2} \rho v^2, \tag{16}$$

where A is the projection of area of the object normal to the velocity, and C_D is a dimensionless constant. Empirical results for a flat circular disk normal to the streamlines show that C_D as a function of R is constant at a value of 1.12 starting at $R \approx 200$ and extending over at least five decades.[7,8] We are now in a position to analyze the data, following the description in Sec. IV.

VI. RESULTS

An examination of the linear fits to the raw velocity versus time data reveals a systematic error for the slope. For larger pieces of cardboard, and hence larger air drag, the slope of the fit deviates more and more from the theoretical prediction of $g \sin \theta$, for reasons discussed in Sec. IV. For the data presented in this paper, the air track was shimmed up 0.0254 m at a distance of 2.283 m from the point where the other end of the air track rested on the table. Therefore, $g \sin \theta$ for this experiment was 0.1091 ± 0.0004 m/s^2. The average slope of the velocity versus time graphs ranged from 0.106 ± 0.002 m/s^2 when no cardboard was on the cart to 0.134 ± 0.010 m/s^2 for the case where the largest (0.0600-m^2) piece of cardboard was used. The systematic nature of this ''error'' can be noted by classes that take data for a range of cardboard areas. If only one size cardboard is used, students can be asked to predict the direction of the expected deviation of fitted slope from ideal. Guiding students to recognize and examine the effects of systematic errors is a valuable exercise.

Given the high Reynolds number that characterizes the cardboard-on-air-cart motion, we can eliminate one fitting parameter for the deviation from ideal velocity curve fit—the exponent D in Eq. (12). If the drag (force) is proportional to the velocity squared, then the deviation of the velocity from the ideal will vary as $|v_{\text{ideal}}|^3 - |v_0|^3$. [See Eqs. (5)–(8).] Data were collected for circular cardboard disks having areas ranging from 6.0×10^{-2} m^2 down to 2.5×10^{-3} m^2. These data were transformed, as described in Sec. IV, and the resulting curve of deviation from ideal velocity versus ideal velocity was fit using the equation

$$y = B * abs(x + C)^3 + E. \tag{17}$$

The average (for 4 to 12 trials) of the cubic coefficient, B, was then plotted as a function of the area of the cardboard disk. The results are shown by the open circles in Fig. 4.

Comparing Eqs. (5) and (16), we see that for the air resistance on the circular disk and $n = 2$

$$b = \tfrac{1}{2} \rho C_D A, \tag{18}$$

so the relationship between b' and A is given by

$$b' = \frac{\tfrac{1}{2} \rho C_D}{(n + 1) m g \sin \theta} A. \tag{19}$$

In the experiment reported here the mass varied with area due to the increased size of the cardboard and the counterweights. The mass of the air track cart was 0.2116 kg and the mass of the 0.060-m^2 cardboard disk was 0.054 kg plus an equal mass in the counterweight. Thus the total mass can be written as $m = 0.2116 \text{ kg} + 0.108 \text{ kg} * A / 0.060 \text{ m}^2$. Combining the expression for the mass with values for the other parameters in Eq. (19) ($\rho = 1.2$ kg/m^3, $C_D = 1.12$, $n = 2$, and $g \sin \theta = 0.11$ m/s^2) we find $b' = 8.8 A / (1 + 8.5 A)$. This equation, with no adjustable parameters, is plotted as curve (a) in Fig. 4. The theoretical curve falls far short of the experimental values.

In order to understand the disagreement between theory and data seen here we might turn to the results of Basano and Ottonello,[5] but the largest disk used in my experiment had just over half the area of their smallest disk, for which the effective mass and history integral were small. Thus we must look for other drag effects that are coming into play. One of
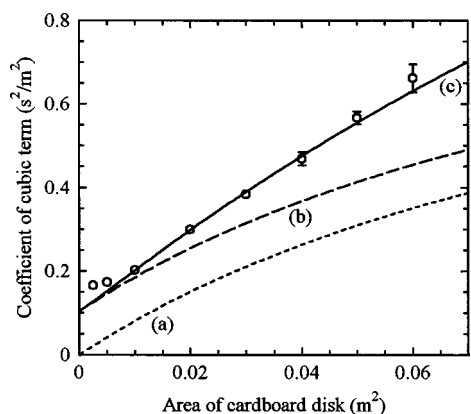
Fig. 4. Average cubic coefficient B from curve fits as in Fig. 3 versus area (circles); theoretical result for air drag on disk only, curve (a), given by $8.8x/(1+8.5x)$; fit including air drag on disk and on cart, curve (b), given by $8.8x/(1+8.5x)+c$, where $c=0.104$ s^2/m^2; fit including air drag on disk, on cart, and effect due to tilting the cart, curve (c), given by $8.8x/(1+8.5x)+c+d*x* \mathrm{sqrt}(x/\pi)/(1+8.5x)$, where $c=0.104$ s^2/m^2 and $d=32.2$ m·s^2.

these effects is present even in the limit $A \to 0$. As the cart moves along the air track the plates that make up the cart experience air drag. Thus we expect a contribution to the drag proportional to the square of the velocity, which is independent of the area of the cardboard. This explains why the experimental curve in Fig. 4 does not go through the origin.

But a simple upward shift of curve (a) in Fig. 4 will not provide a good fit to the data, as can be seen by looking at curve (b). Another effect must be making a measurable contribution. The circular disk experiencing the air drag given by Eq. (16) is placed with its center above the line passing through the center of mass of the air cart. (The diameter of the disks makes this inevitable, or they would run into the air track.) Thus the air drag produces a torque on the cart. Whether the cart is going up or down the air track, the torque is in a direction to tilt the leading end of the cart up off the track slightly. A slight tilt in the cart relative to the air track should cause an additional air resistance contribution, this time due to the air jets from the air track exerting a small component of force that is not perpendicular to the air cart plates. In fact, whether traveling up or down the incline the tilt from the torque on the disk causes this non-normal force to oppose the motion of the cart. This force from the air jets will vary linearly with the tilt angle (since it is small) and hence with the torque. Because the velocity of the air from the jets is far greater than the velocity of the cart relative to the air track, the latter velocity does not need to be considered, except in determining the tilting torque. We can include this type of effect in our fitting equation by noting that the torque will depend linearly on the product of F_D, which is proportional to $A/(1+8.5A)$, and the moment arm. The moment arm is the diameter of the circular disk, $(A/\pi)^{1/2}$, plus the distance from the mounting point to the line parallel to the air track passing through the center of mass of the cart. In my case this distance was less than 0.001 m and hence negligible. The term in the fitting equation corresponding to the tilt effect is given by

$$dA\frac{(A/\pi)^{1/2}}{1+8.5A}, \qquad (20)$$

where d is the only adjustable parameter.

Combining the air drag from the disk, the air drag from the sides of the cart, and the tilt effect, we have an equation with two adjustable parameters with which to fit the experimental data:

$$y=8.8x/(1+8.5x)+c+dx(x/\pi)^{1/2}/(1+8.5x). \qquad (21)$$

The best fit, made without using the two smallest areas, is shown as a solid line [curve (c)] in Fig. 4. The two smallest areas were not used because the scatter in the $v-v_{\mathrm{ideal}}$ vs v_{ideal} graph was so large that the cubic coefficients obtained are highly uncertain, even though multiple runs were averaged. The relative contribution of the three phenomena can be seen by comparing curve (a), which represents the first term in Eq. (21), curve (b), which represents the first two terms in Eq. (21), and curve (c), which contains all three terms. The final fit that takes into account all three effects described involves only two fitting parameters. After so many manipulations of the data and so much amplification of the noise it is gratifying to see a clear pattern emerge in the result that can be explained by simple physics.

A word is in order about the use of circular pieces of cardboard. This experiment was first run using rectangular pieces of cardboard, but the best curve fits for the deviation from ideal velocity curves had exponents on the velocity clustered around 2 instead of 3. Behavior of drag on a bluff object as discussed in fluid mechanics books seems to be limited to circular disks. Perhaps the corners of the cardboard affect the symmetry of the flow in a way that is significant. The quiescent region behind the disk may not exist to the same extent behind a rectangular plate. If so, the pressure difference on the two sides may not be the simple $\frac{1}{2}\rho v^2$ as holds for the disk. Based on the authoritative fluid dynamics texts and personal experience, I recommend against using rectangular cardboard sheets to provide air resistance.

VII. SUMMARY

The air track and the motion sensor are two ubiquitous pieces of physics laboratory equipment. Together with a simple plotting package, these tools can be used to allow students to explore the nonideal nature of the ''frictionless'' air track. The benefits of this exercise are numerous, for both the introductory and more advanced physics student: The notions of simple motion with (roughly) constant acceleration are reinforced. An acknowledgment of the deviations from ideal behavior is made. A systematic study of what is generally classified simply as ''noise'' is carried out, to the point of fitting the ''noise'' with a simple curve. The more advanced uses of plotting packages are introduced. Some simple concepts of air resistance are explored empirically. As is so often the case, we must look beyond the simple explanations to find all the pieces of the physics puzzle, but when we do, the results are satisfying.

ACKNOWLEDGMENTS

[1]Stuart Karon, *Easyplot*™ (Spiral Software, Brookline, MA, 1997).

[2]Christopher Brueningsen *et al.*, ''Modeling air drag,'' Phys. Teach. **32**, 439–441 (1994); Vasilis Pagonis *et al.*, ''Effects of air resistance,'' *ibid.*

[35], 364–368 (1997); Margaret Greenwood *et al.*, ''Air resistance acting on a sphere: numerical analysis, strobe photographs, and videotapes,'' *ibid.* **24**, 153–159 (1986).

[3] G. Wagner and R. Wood, ''Skydiver survives death plunge (and the physics that helped),'' Phys. Teach. **34**, 543 (1996).

[4] John E. Farr, ''Determining the air drag on a car,'' Phys. Teach. **21**, 320–321 (1983); Joseph M. Zayas, ''Experimental determination of the coefficient of drag of a tennis ball,'' Am. J. Phys. **54**, 622–625 (1986); William Keig, ''Velocity dependence of friction on an air track,'' Am. J. Phys. **53**, 1084 (1985).

[5] L. Brasano and P. Ottonello, ''The air drag on an accelerating disk: A laboratory experiment,'' Am. J. Phys. **57**, 999–1004 (1989).

[6] Raymond A. Serway, *Physics for Scientists and Engineers*, 4th ed. (Saunders, Philadelphia, 1996); Hugh D. Young, *University Physics*, 8th ed. (Addison Wesley, Reading, MA, 1992); Eugene Hecht, *Physics (Calculus)* (Brooks-Cole, Belmont, MA, 1996).

[7] T. E. Faber, *Fluid Dynamics for Physicists* (Cambridge U.P., New York, 1995), p. 231.

[8] G. K. Batchelor, *Fluid Dynamics* (Cambridge U.P., New York, 1967), p. 339.

HANG ALL THE PROFESSORS

After sober and judicious consideration, and weighing one thing against another in the interests of reasonable compromise, H. L. Mencken concluded that a startling and dramatic improvement in American education required only that we hang all the professors and burn down the schools. His uncharacteristically moderate proposal was not adopted. Those who actually knew more about education than Mencken did could see that his plan was nothing more than cosmetic and would in fact provide only an outward appearance of improvement. Those who knew less, on the other hand, had somewhat more elaborate plans of their own, and they just happened to be in charge of the schools.

Richard Mitchell, *The Graves of Academe* (Little, Brown and Company, Boston, 1981), p. 69.